53rd AIAA/ASME/ASCE/AHS/ASC Structures, Structural Dynamics and Materials Conference<BR>20th AI
23 - 26 April 2012, Honolulu, Hawaii

AIAA 2012-1881

# SDM 2012 Student Papers Competition

# Design and Analysis of Dual Pressure Probes for Predicting Turbulence-Induced Vibration in Low Velocity Flow

Jared D. Hobeck* and Daniel J. Inman†

*Department of Aerospace Engineering, University of Michigan, Ann Arbor, MI, 48109, USA*



**Measuring highly turbulent fluid flow is challenging, especially in cases where the turbulence intensity exceeds acceptable limits for hotwire anemometry techniques. Using fast response pressure probes is an effective and well documented turbulence measurement method; however, there is little literature about pressure probes capable of measuring turbulence in low mean velocity air flows (0-12 m/s). Also lacking in the literature is a complete method of using pressure probe measurements to predict turbulence-induced vibration. In this paper the design and analysis of two high-sensitivity pressure probes is discussed. It will be shown how measurements with these probes are used to develop a statistically derived turbulent fluid forcing function. This function will then be combined with an analytical structural dynamics model such that not only the modal RMS displacements, but also the modal displacement power spectral density plots can be predicted for a given structure. The pressure probe design, turbulence measurement techniques, and both the statistical and analytical models will be validated with experimental results. The results shown in this paper are for a case study performed with a single cantilever exposed to turbulent cross-flow.**

## Nomenclature

$A$ = cantilever area normal to flow
$F_f$ = distributed fluid force
$H$ = complex frequency response function
$J_{rs}$ = acceptance integral term
$L$ = cantilever length
$R$ = cross-correlation
$S$ = power spectral density
$YI$ = bending stiffness of cantilever
$c_a$ = coefficient of viscous fluid damping
$c_s$ = coefficient of viscoelastic strain-rate damping
$j$ = imaginary number
$m$ = linear mass density
$r, s$ = integer subscripts that denote a particular mode of vibration
$p$ = dynamic pressure
$w$ = transverse beam deflection

* Ph.D. Pre-candidate, Department of Aerospace Engineering , University of Michigan, 1320 Beal Avenue, Ann Arbor, MI, 48109, Mail Code 2140, AIAA Member

† Chair and "Kelly" Johnson Collegiate Professor, Department of Aerospace Engineering , University of Michigan, 1320 Beal Avenue, Ann Arbor, MI, 48109, Mail Code 2140, AIAA Fellow

$x$ = streamwise coordinate axis
$z$ = cantilever span coordinate
$\zeta_r$ = modal damping ratio
$\eta_r$ = modal displacement
$\phi_r$ = structural mode shape function
$\psi_r$ = modal turbulence-induced forcing function

## I. Introduction

TURBULENT or highly unsteady fluid flows are abundant in nature and are commonly encountered in real-world engineering applications. When elastic structures are exposed to turbulent flow, turbulence-induced vibration (TIV) is inevitable. In many cases TIV is problematic, and can cause catastrophic structural damage. In other cases, such as energy harvesting applications for example, one may wish to maximize vibration caused by turbulence.[1,2] Regardless of the application, the most challenging aspect of understanding and modeling turbulence-induced vibration is that turbulent flows are both unpredictable and difficult to measure. Therefore, the motivation behind this work is not only to present an effective method of turbulence measurement, but also to show how these measurements can be used to predict turbulence-induced vibrations. The modeling techniques developed in this work could then be used to modify the design of any structure to allow only desired levels of turbulence-induced vibration.

Motivation for this work began during a recent investigation of energy harvesting methods in low velocity flows with high-intensity turbulence.[1,2] Many authors have explored energy harvesting techniques for flow-induced vibration; however, all modeling methods found in the literature are based on either vortex induced vibration[3,4], or flutter[5,6]. An experimental study was performed on energy harvesting from vibration caused by boundary layer turbulence[7]; however, energy harvesting from TIV caused by large scale turbulence remained absent from the literature. Although an energy harvesting study inspired the work presented here, this paper focuses on the TIV modeling details which proved to be a necessary and interesting aspect of the energy harvesting research.

Extensive efforts have been put toward the development of fast response pressure probes for measuring turbulent flow. Work done by Jezdinsky (1966) is among the earliest discussed in literature on the topic of measuring turbulent flows with pressure probes.[8] The majority of research on this topic has been developed for high velocity turbulent flow environments such as those encountered in turbomachinery.[9–12] The work presented in this paper, however, is to make measurements and predictions based on low-velocity turbulent flows such as those found in ventilation systems, slow moving vehicles, or natural environments i.e., wind and streams.

The proposed turbulence-induced vibration model is a modification of a model first developed by Powell (1958),[13] and used extensively by Au-Yang[14,15]. This original model was only applied to direct measurement techniques where pressure fluctuations are measured by arrays of transducers fixed on the surface of the structure. Direct measurement techniques could not be implemented in the current study because fixing an array of transducers to the structure surface would greatly modify or hinder the true turbulence-induced vibration response.

Indirect measurement methods have also been explored, and are discussed in the literature. Indirect measurement refers to a process where the free stream turbulence is measured using hotwire anemometry, pressure probes, or other techniques and the dynamic response of a structure placed in that flow can be approximated. Research done by Grover *et al.* (1978) shows extensive experimental analysis of tube bank dynamics where hotwire probes were used to measure the turbulence spectra.[16] Later, Axisa *et al.* (1990) performed both theoretical and experimental analyses on turbulent excitation of tubes in cross-flow.[17]

The technique presented in this paper combines *indirect* turbulence measurements with the previously discussed *direct* model approach. The primary advantage to the proposed method is that it is easy to implement, yet still provides very accurate predictions compared to existing techniques. Another key advantage is that after the turbulence is measured, predictions can be made for any structure experiencing similar flow conditions. These advantages along with other performance metrics, calibrations, and a detailed model are discussed in this paper.

## II. Mathematical Model

Due to the unpredictable nature of high-intensity turbulent flow, the most practical approach toward developing a turbulent fluid forcing function is to employ statistical techniques. The full model consists of an analytical structural dynamics portion which will be combined with a statistically derived forcing function. In order to maintain the focus of this modeling approach on the development of a turbulent forcing function, a simple Euler-Bernoulli cantilever beam will be used as the analytical structural component (figure 1). It is important to note, however that this model can easily be adapted to accommodate more complex structures.

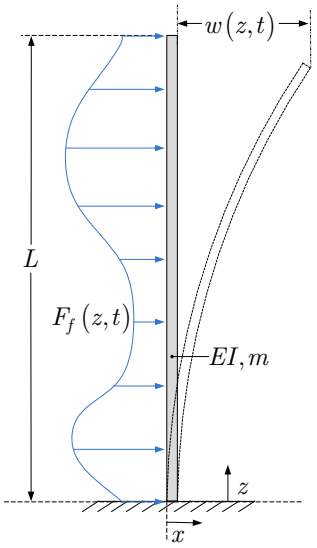


**Figure 1. Cantilevered Euler-Bernoulli beam subject to a distributed turbulence-induced fluid force**

### A. Preliminaries on Spectral Statistics

For the proposed model, the measured pressure $p(t)$ is assumed to be a stationary random process in which its mean, mean square, variance, and standard deviation do not change with time.[18] Turbulence measurements performed for this work were recorded as time-series pressure data. It is necessary therefore, to perform several statistical operations which reduced the raw data into more useful and meaningful forms. The correlation function is a measure of how similar the pressure varies with time at two points in space (say $z_1$ and $z_2$). The pressure cross-correlation can be given as

$$R_p(z_1, z_2, \tau) = \lim_{T\to\infty}\left(\frac{1}{2T}\right)\int_{-T}^{T} p(z_1,t)p(z_2,t+\tau)dt \tag{1}$$

where $T$ is the sample time period and $\tau$ is a shift in time $t$ between the two pressure signals. Another statistical measure used commonly in this analysis is called the pressure cross power spectral density (CPSD). The pressure CPSD is a measure of energy content within a signal and how it is distributed across the entire frequency spectrum of interest. Simply by taking the Fourier transform of the cross-correlation function one can get the following expression for the CPSD

$$S_p(z_1, z_2, \omega) = \lim_{T\to\infty}\frac{1}{4\pi T}\int_{-\infty}^{\infty}\left[\int_{-T}^{T} p(z_1,t)p(z_2,t+\tau)dt\right]\mathrm{e}^{-j\omega t}d\tau \tag{2}$$

where $j$ is the imaginary number and $\omega$ is angular frequency in rad/s. It is important to note that throughout this paper $S_p$ is referred to as the double-sided CPSD function with units $\mathrm{Pa}^2$/rad/s.

### B. Analytical Model

This portion of the model defines the structural dynamics equations and how they are coupled with the turbulence-induced forcing function. The simple case presented here is modeled as a cantilever beam subject to a distributed turbulence-induced fluid force along its length and normal to its surface as illustrated in figure 1.

In this analysis it is assumed that the beam is a long, slender, rectangular, cantilever experiencing small transverse deflections. Provided the previous assumptions hold true, the beam can be modeled using the well-known Euler-Bernoulli beam equations. The governing differential equation of motion for a beam subject to a distributed force can be expressed as

$$YI\frac{\partial^4 w(z,t)}{dz^4} + c_s I\frac{\partial^5 w(z,t)}{dz^4 dt} + m\frac{\partial^2 w(z,t)}{dt^2} + c_a\frac{\partial w(z,t)}{dt} = F_f(z,t) \tag{3}$$

where, $w(z,t)$ is the transverse beam deflection, $Y$ is the Young's modulus of the beam, $c_s$ is the coefficient of viscoelastic strain rate damping, $I$ is the beam area moment of inertia, $m$ is the linear mass density, $c_a$ is the coefficient of viscous damping, and $F_f(z,t)$ is an arbitrary distributed transverse load along the

length of the beam. Assuming that the solution can be expressed as a infinite and convergent series, the relationship between steady state modal displacement $\eta_r$, and a modal distributed fluid force $\psi_r$ can be expressed as

$$\eta_r(t) = \frac{\psi_r e^{j\omega t}}{m_r(\omega_r^2 - \omega^2 + j2\zeta_r\omega_r\omega)} = H(\omega)\psi_r e^{j\omega t} \tag{4}$$

where the subscript $r$ denotes the mode number, $\omega_r$ is the natural frequency, $H$ is the complex frequency response function, and the damping terms in equation (3) can be combined to give one modal damping parameter $\zeta_r$. Upon performing the general procedure of substituting the assumed solution into equation (3), multiplying by the mode shape $\phi_r$, integrating over beam length $L$, and taking the Fourier transform one can attain the following.

$$\psi_r(z,t) = \int_{-\infty}^{\infty}\int_0^L \phi_r(z)F_f(z,t)\mathrm{e}^{-j\omega t}dzdt \tag{5}$$

Equation (5) is an expression for the modal forcing term due to an arbitrary distributed force. Analytical solutions for predicting the velocity or pressure field within a highly turbulent flow do not exist. Therefore, the time-domain forcing function $F_f(z,t)$ cannot be defined, and either statistical or numeric methods must be used to develop a modal forcing function $\psi_r$.

### C. Statistical Model

Using classic random vibration theory, one can express the mean-square amplitude of a single degree of freedom oscillator subject to a random forcing function as[18]

$$\overline{x}^2 = \int_{-\infty}^{\infty} S_x(\omega)\,d\omega = \int_{-\infty}^{\infty} \left|H(\omega)\right|^2 S_{\mathrm{f}}(\omega)d\omega \tag{6}$$

where $S_x$ is the displacement power spectral density (PSD) of the system, $S_f$ is the forcing function PSD, and $H$ is the complex frequency response function of the oscillator. A similar approach is taken for the distributed parameter system and is discussed in this section.

The most difficult aspect of predicting turbulence-induced vibrations is estimating the PSD of the distributed forcing function $S_f$. Powell (1958) developed a technique for estimating turbulence-induced vibration called the acceptance integral method. The acceptance integral is a measure of how effective a turbulent force is at exciting particular dynamic modes of a structure. One form of the acceptance integral can be expressed as[13]

$$J_{rs}(\omega) = \frac{1}{LS_p(z_0,\omega)}\int_0^L\int_0^L \phi_r(z)S_p(z,z',\omega)\phi_s(z')dzdz' \tag{7}$$

where $J_{rs}$ is the acceptance term, $L$ is the beam length, $S_p$ is the pressure cross-power spectral density (CPSD) along the length of the beam, and both $z$ and $z'$ are arrays of points along the z-axis. Figure 2 shows theoretical trends of the acceptance for the first three modes of a cantilever beam. An idealized expression for the coherence function as discussed by Au-Yang (2000) was used to evaluate the acceptance integral as a function of *correlation length* $\lambda$. The plots in figure 2 can be regarded as upper bounds of the acceptance value where a perfectly correlated turbulent force along the length of the beam causes $\lambda \Rightarrow \infty$ conversely, a poorly correlated force causes $\lambda \Rightarrow 0$. Given that an expression for the acceptance can be attained, the total displacement PSD of a cantilever beam can then be expressed as[15]

$$S_w(z,\omega) = A\sum_{r=s}^{\infty}\phi_r(z)^2\left|H_r(\omega)\right|^2 J_{rr}(\omega) + 2A\sum_{r\neq s}^{\infty}\phi_r(z)\phi_s(z)H_r(\omega)^* H_s(\omega)J_{rs}(\omega) \tag{8}$$

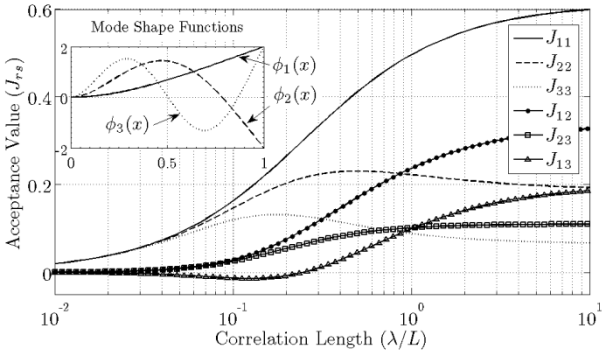


**Figure 2. Theoretical cross and joint acceptance for first three modes of a cantilever beam.**

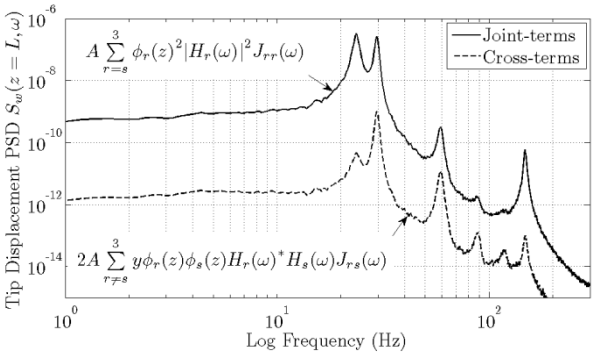


**Figure 3. Comparison of tip displacement contributions between joint and cross acceptance terms.**

Where $A$ is the area of the cantilever normal to the turbulent flow, and $H_r$ is the modal complex frequency response function for the structure as defined in equation (4)[‡]. In many cases it can be shown that the amplitudes of vibration associated with the cross-terms $(m \neq n)$ in equation (8) are significantly less than those for the joint terms ($m$=$n$). Assuming that the joint terms are negligible, the total displacement PSD of the cantilever beam becomes

$$S_w(z,\omega) = A\sum_{r=1}^{\infty}\phi_r(z)^2\left|H_r(\omega)\right|^2 J_{rs}(\omega) \tag{9}$$

For the remainder of this analysis it is assumed that the cross terms are negligible. This assumption is experimentally justified in the case study results from figure 3, where the tip displacement PSD contribution from cross acceptance terms is approximately 2 orders of magnitude less than that of the joint acceptance terms at all frequencies. Because RMS displacement is a function of the integral of the PSD as shown in equation (6), one can conclude that the cross term contributions are indeed negligible.

### D. Combined Turbulence-Induced Vibration Model

Similar to a single degree of freedom system, the mean square displacement of the cantilever is found by integrating the displacement PSD over the frequency range. The modal mean square displacement can then be expressed as,

$$\overline{w}_r^2(z) = A\int_{-\infty}^{\infty}\phi_r(z)^2\left|H_r(\omega)\right|^2 J_{rr}(\omega)d\omega \tag{10}$$

where the overbar on $w$ denotes a time-averaged value. By removing the mode shape terms from equation (10) and assuming a sinusoidal response, it can be shown than the mean modal displacement can be attained with the following expression.

$$\eta_r = \left[2A\int_{-\infty}^{\infty}\left|H(\omega)\right|^2 J_{rr}(\omega)d\omega\right]^{\frac{1}{2}} \tag{11}$$

It is now straightforward to express the total cantilever displacement as

$$w(z,t) = \sum_{r=1}^{\infty}\phi_r(z)\eta_r(t) = \sum_{r=1}^{\infty}\left\{\left[2A\int_{-\infty}^{\infty}\left|\frac{1}{m_r(\omega_r^2-\omega^2+j2\zeta_r\omega_r\omega)}\right|^2 J_{rr}(\omega)d\omega\right]^{\frac{1}{2}}\phi_r(z)\mathrm{e}^{j\omega t}\right\} \tag{12}$$

[‡] The asterisk (*) in equation (8) denotes the complex conjugate of the frequency response function.

where one can immediately see that an attractive feature of this model is that only the acceptance terms ($J_{rr}$) are statistically determined. All other parameters of the cantilever (or structure of interest) can be chosen according to desired or allowable levels of vibration.

## III. Pressure Probes

Two high sensitivity pressure probes were designed and built for the measurement of fluctuating dynamic pressure within highly turbulent, low-velocity flow. Pressure transducers and pitot tubes were preinstalled in the wind tunnel where the experiments were performed; however, they could not be used due to their lack of bandwidth and sensitivity. Because of the extremely high turbulence intensities (>25%), hotwire anemometry could not provide reliable velocity measurements.[19]

Each probe consists of a MEMS-based differential pressure sensor enclosed such that one port is exposed directly to turbulent flow while the other is isolated within a breathable chamber. This chamber consists of rigid walls with portions of thick cloth which act as a buffer for the static port to insure fluctuating pressures are measured at the dynamic port only. The pressure sensor in each probe has a differential pressure range of $\pm 249$ Pa with a dynamic response time of $\leq 100\,\mu$s (All Sensors Corp. Model1-INCH-D-MV). Design details of the probes are listed in table 1, while a schematic and photo of the probes is shown in figure 4.

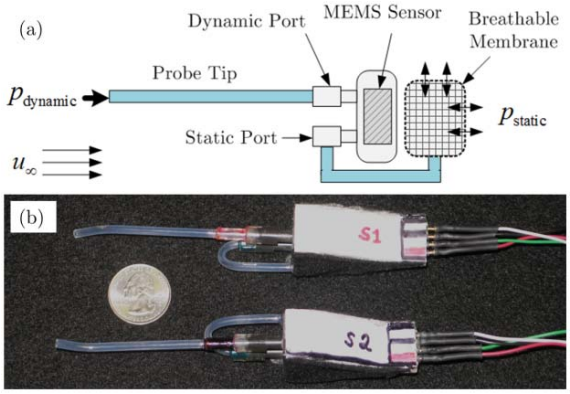


**Figure 4. Schematic (a) of pressure probe design and a photo (b) showing the two probes used to perform turbulence measurements for the statistical model.**

**Table 1. Pressure probe design parameters.**

| | | |
|---|---|---|
| Probe diameter | 1.52 | mm |
| Tip length | 9.27 | cm |
| Static port length | 9.27 | cm |
| Sensor volume | 240 | $mm^3$ |
| Pressure range | $\pm 249$ | Pa |
| Bandwidth | 300 | Hz |
| Output voltage range | $\pm 16$ | mV |

### A. Calibration Methods

Both static and dynamic calibrations were performed on the pressure probes. For both calibration types, the probe tips were oriented normal to the mean velocity flow direction. Static calibration refers to low turbulence intensity (<1%) flow measurement where only the average sensor voltage output is recorded at each velocity interval. Results of the static calibrations are shown in figure 5.

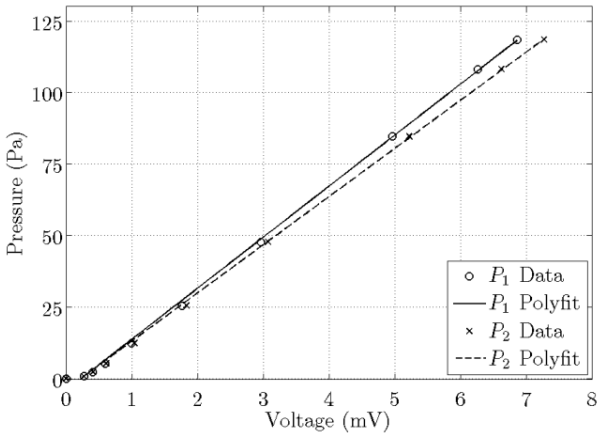


**Figure 5. Static calibration results for both pressure probes showing very similar and linear responses.**

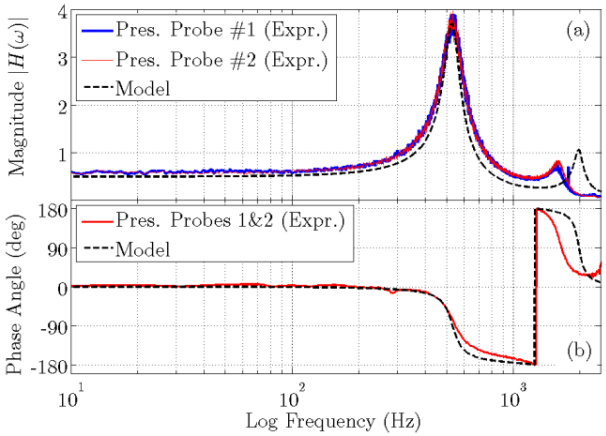


**Figure 6. Experimental and theoretical results of the dynamic response characteristics for both pressure probes showing acoustic attenuation (a) and phase distortion (b).**

The dynamic response characteristics of each probe were found using a noise excitation system identification method. This method was used for a similar analysis performed by both Lenherr *et al.* (2011)[9] and Ommen *et al.* (1999)[20]. The reference excitation was grid turbulence having an intensity of 10% which was measured with the pressure probes and a hotwire probe simultaneously. The hotwire measurements were used as reference inputs to the system, while corresponding pressure probe measurements were used as outputs. The frequency response measurement results are shown in figure 6.

### B. Dynamic Response Model

Extensive modeling techniques performed on various pneumatic tube and transducer configurations can be found in literature. A model presented by Bergh and Tijdeman (1965) was used to predict the dynamic acoustic response characteristics of both pressure probes.[21] Each probe was designed to have enough bandwidth and sensitivity to accurately measure pressure fluctuations within the frequency range of the first and second natural frequencies of the structures to be tested (approximately 300 Hz). The bandwidth limit was set based on preliminary experimental results that showed no significant structural displacement amplitudes were present from the second mode and higher. Results of the model shown in figure 6 demonstrate good agreement between experiment and theory. These results also show that the desired bandwidth target was successfully attained.

## IV. Experimental Methods & Model Validation

Both the measurement techniques and the turbulence-induced vibration model were experimentally validated by performing two case studies. Procedures and results of these studies are presented in this section.

### A. Turbulence Measurements

Without the cantilever present, a series of incremental pressure probe measurements were made in turbulent flow generated by placing a bluff body in a wind tunnel. Figure 7 illustrates the pressure probe measurement locations relative to where the cantilever would later be positioned. Data from these measurements was processed using the previously discussed statistical modeling techniques. The pressure coherence function can be considered as a type of normalized PSD function and is defined as

$$C_p(z,z',\omega) = \frac{S_p(z,z',\omega)}{S_p(z,\omega)} \tag{13}$$

which is simply the *cross* power spectral density normalized by the power spectral density. The coherence profile measured in this case study is shown in figure 8 where the probe separation (*y-axis*) corresponds directly to the probe locations given in figure 7.

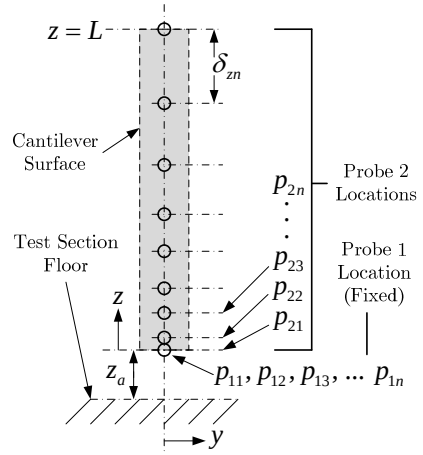


**Figure 7. Schematic of pressure probe measurement locations relative to the cantilever surface.**

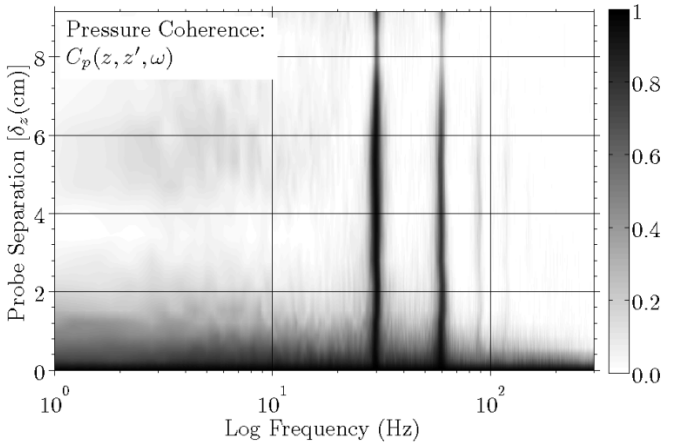


**Figure 8. Pressure coherence profile results from pressure probe measurements.**

The first dark vertical band in the coherence plot (figure 8) clearly shows the primary vortex shedding frequency of the bluff body that was used to create the turbulence.

The goal of these measurements was to develop a turbulence profile where both spatial and spectral information was gathered. After the turbulence profile is computed, the modal turbulence-induced force exerted on the cantilever could be predicted. The modal forcing function was then applied to the cantilever and the displacement PSD was calculated using the full model given in equation (12).

Each pressure probe was powered with 16 VDC and had an output range of $\pm 16$mV providing a pressure sensitivity of 0.064 mV/Pa. Siglab data acquisition hardware was used to simultaneously power the sensors and measure their output. The time series voltage output from each probe was sampled at 5.12 kHz with a sample size of $2^{21}$ samples. The duration of each test was approximately seven minutes. At the end of each test, probe-2 was repositioned and the procedure was repeated at a total of 16 locations along the $z$-axis.

### B. Case Study Results

Two case studies were performed to experimentally validate the full turbulence-induced vibration model. The acceptance integrals were calculated for the first three modes of vibration using the pressure coherence profile shown in figure 8 in conjunction with equation (7). Plots of the acceptance integrals are given in figure 9. As expected, the acceptance associated with the first bending mode of the cantilever ($J_{11}$) was the largest. Table 1 summarizes the design parameters and results of each case.

**Table 2. Cantilever design parameters and case study results**

| Case | Material | Length (cm) | Width (cm) | Thick. ($\mu$m) | Natural Freq. (Hz) 1st mode | Natural Freq. (Hz) 2nd mode | RMS Tip Disp. (mm) Expr. | RMS Tip Disp. (mm) Model | Error (%) |
|---|---|---|---|---|---|---|---|---|---|
| #1 | Steel | 8.64 | 2.54 | 254 | 25.5 | 160.1 | 1.313 | 1.285 | 2.20 |
| #2 | Composite | 9.40 | 2.54 | 508 | 41.9 | 175.6 | 0.566 | 0.597 | -4.99 |

The two cantilevers of similar size were designed such that their fundamental mode frequencies and complex response functions were different from each other and from the primary vortex shedding frequency within the turbulent flow spectrum. By separating these known frequencies of interest, the model's ability to capture both fluid forcing effects and structural dynamics could be demonstrated. Results of both the tip displacement PSD shown in figure 10 and RMS tip displacement listed in table 2 show very good agreement between model predictions and experimental measurements.

Pressure coherence and PSD are two forms of the turbulence profile produced from spectral analysis of the pressure probe data. Applying slightly different forms of the full model, identical displacement PSD results can be achieved by using either the coherence function or the pressure PSD function. The results shown in figure 10 were produced using the pressure coherence function. For case-1 the first and second

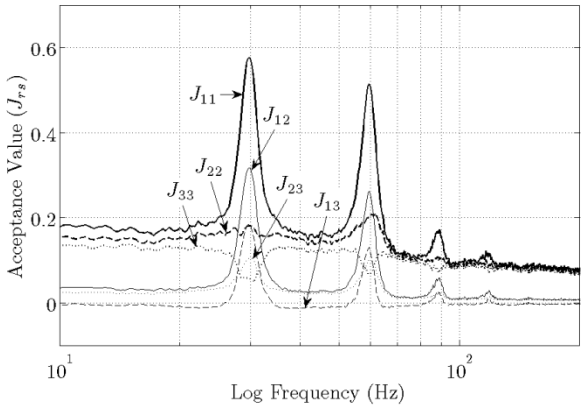


**Figure 9. Joint and cross-acceptance values calculated from pressure probe data used for formulating a turbulence-induced modal forcing function.**

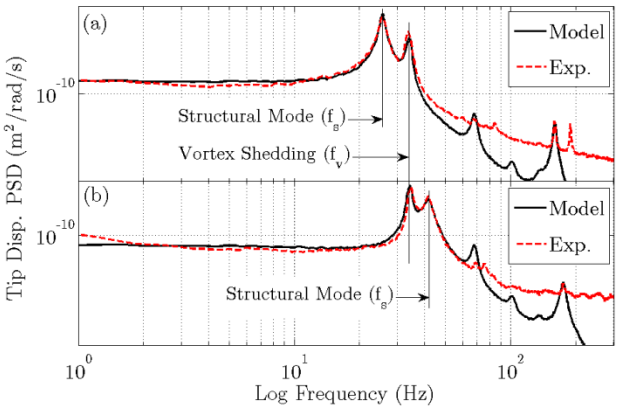


**Figure 10. Tip displacement PSD functions comparing model results to experimental measurements for case-1 (a) and case-2 (b).**

peaks are associated with the first mode of the cantilever and the primary vortex shedding frequency respectively. The opposite is true for case-2. The primary vortex shedding frequency is 33.7 Hz.

## V. Conclusions

The modeling and turbulence measurement techniques presented in this paper are shown to be quite effective at predicting turbulence-induced vibrations. Pressure probes were designed and constructed such that they were able to measure turbulent air flow with a full pressure range of $\pm 249$ Pa, a bandwidth of approximately 300 Hz, and a sensitivity of 0.064 mV/Pa. Successful modeling and calibration methods were applied to the pressure probes to ensure reliable measurements even in highly turbulent air flow with a mean velocity range of only (0-12 m/s). Results of two case studies show that the turbulence-induced vibration predictions agree well with those measured in experiments. The largest error associated with predicting RMS tip deflection was found to be slightly less than 5%.

## Acknowledgments

The authors would like to extend their sincere acknowledgements to Science Applications International Corporation for funding this research through the NSF I/UCRC Center for Energy Harvesting Materials and Systems at Virginia Tech and to the University of Michigan College of Engineering.

## References

[1]Hobeck J D and Inman D J , 2012, Artificial Piezoelectric Grass for Energy Harvesting from Turbulence-induced Vibration *Smart Materials and Structures*. (in press)

[2]Hobeck J D and Inman D J , 2011, Energy Harvesting From Turbulence-Induced Vibration in Air Flow: Artificial Piezoelectric Grass Concept *ASME Conference Proceedings*, **2011**, 637–646.

[3]Bernitsas M M , Raghavan K , Ben-Simon Y , Garcia E and others, 2008, Vivace (vortex induced vibration aquatic clean energy): A new concept in generation of clean and renewable energy from fluid flow *Journal of Offshore Mechanics and Arctic Engineering*, **130**, 041101.

[4]Hobbs W B and Hu D L , 2012, Tree-inspired piezoelectric energy harvesting *Journal of Fluids and Structures*, **28**, 103 - 114.

[5]Dunnmon J , Stanton S , Mann B and Dowell E , 2011, Power extraction from aeroelastic limit cycle oscillations *Journal of Fluids and Structures*.

[6]Erturk A , Vieira W , De Marqui Jr C and Inman D , 2010, On the energy harvesting potential of piezoaeroelastic systems *Applied physics letters*, **96**, 184103.

[7]Akaydin H D , Elvin N and Andreopoulos Y , 2010, Energy harvesting from highly unsteady fluid flows using piezoelectric materials *Journal of Intelligent Material Systems and Structures*, **21**, 1263.

[8]Jezdinsky V , 1966, Measurement of Turbulence by Pressure Probes *AIAA Journal*, **4**, 2072.

[9]Lenherr C , Kalfas A I and Abhari R S , 2011, High temperature fast response aerodynamic probe *Journal of Engineering for Gas Turbines and Power*, **133**, 011603.

[10]Shepherd I C , 1981, A Four Hole Pressure Probe for Fluid Flow Measurements in Three Dimensions *Journal of Fluids Engineering*, **103**, 590.

[11]Hooper J and Musgrove A , 1997, Reynolds stress, mean velocity, and dynamic static pressure measurement by a four-hole pressure probe *Experimental thermal and fluid science*, **15**, 375–383.

[12]Lee S W and Jun S B , 2005, Reynolds number effects on the non-nulling calibration of a cone-type five-hole probe for turbomachinery applications *Journal of mechanical science and technology*, **19**, 1632–1648.

[13]Powell A , 1958, On the fatigue failure of structures due to vibrations excited by random pressure fields *The Journal of the Acoustical Society of America*, **30**, 1130–1135.

[14]Au-Yang M , 1975, Response of reactor internals to fluctuating pressure forces *Nuclear Engineering and Design*, **35**, 361–375.

[15]Au-Yang M , 2000, Joint and cross acceptances for cross-flow-induced vibration-Part II: Charts and applications *Journal of pressure vessel technology*, **122**, 355–361.

[16]Grover L and Weaver D , 1978, Cross-flow induced vibrations in a tube bank-Vortex shedding *Journal of Sound and Vibration*, **59**, 263–276.

[17]Axisa F , Antunes J and Villard B , 1990, Random excitation of heat exchangertubes by cross-flows *Journal of fluids and structures*, **4**, 321–341.

[18]Newland D E , 1975, *An introduction to random vibrations and spectral analysis* (Longman).

[19]Bruun H H , 1995, *Hot-wire anemometry: principles and signal analysis* (Oxford University Press).

[20]van Ommen J R , Schouten J C , vander Stappen M L M and van den Bleek C M , 1999, Response characteristics of probe-transducer systems for pressure measurements in gas-solid fluidized beds: how to prevent pitfalls in dynamic pressure measurements *Powder Technology*, **106**, 199–218.

[21]Bergh H and Tijdeman H , 1965, *Theoretical and experimental results for the dynamic response of pressure measuring systems* (Nationaal lucht-en ruimtevaartlaboratorium).